Article

Topological Entropy Characterization, NMR and ESR Spectral Patterns of Coronene-Based Transition Metal Organic Frameworks

Zahid Raza, Micheal Arockiaraj,* Aravindan Maaran, S. Ruth Julie Kavitha, and Krishnan Balasubramanian

Cite This: *ACS Omega* 2023, 8, 13371−13383

Read Online

| ACCESS | | 📊 Metrics & More | | 📖 Article Recommendations |

ABSTRACT: Metal organic frameworks (MOFs) are topical crystalline materials with high porosity and inner surface areas synthesized from naturally occurring minerals. Such MOFs with transition metals have attracted considerable attention because of their fascinating morphological diversity and tunable characteristics. The coronene-based structural frameworks with transition metal atoms are synthesized by repeating a fixed coronene unit at several levels. In this study, topological indices and NMR and ESR spectral patterns are computed for these MOFs to shed light on their structures and spectral properties. We obtained mathematical expressions of topological indices based on degree and degree-sum values of MOFs for the rectangular, hexagonal, and parallelogram peripheral shapes. Furthermore, the entropy measures of these novel frameworks are evaluated with the help of index functionals and compared to a wide range of degree-based descriptors. The NMR and ESR spectral patterns have been obtained from the distance degree vector sequences and symmetries for the three MOFs.
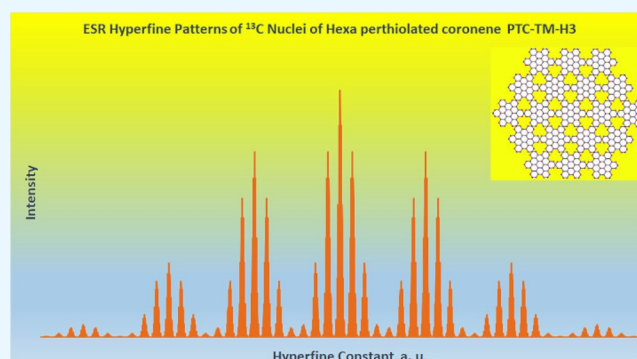
1. INTRODUCTION

Metal organic frameworks (MOFs), composed of metal clusters that are linked with organic linkers, have become increasingly important in recent years[1−3] due to their tunable nature and unusual properties. The MOFs comprise organic ligands, framework topology, and metal centers, which play a vital role in designing the size, shape, and dimensionality of the structure. Their functionality and properties can be tailored by tuning their basic structural units during or even after their synthesis,[2] thus paving the way for multifunctional materials with diverse applications.[4−9] The key characteristic of MOFs is their structural variability that lends to different topologies by simply adjusting their basic building blocks. Consequently, novel materials with tunable properties can be tailor-made by varying their structural topologies.[10] Hence these materials have highly desirable properties for environmental remediation and in sustainable chemistry.[4−6] They have also been employed to enhance the capacity of batteries, build super capacitors,[7] separating inorganic mixtures,[8] and in hydrogen and energy storage applications.[9] In addition, MOFs could be used as precursors for the design of various nanostructures[11,12] and act as potential candidates for anticancer therapy[13] and catalysis.[14]

A drawback of MOFs is their low conductivity due to their varied structures and morphologies.[15] Due to their large surface areas and porous structures, they have better sorption capabilities, opening the door for the synthesis of a plethora of

similar frameworks by altering the transition metals and the linkers.[16] Persulfurated coronene $C_{24}S_{12}$ (PSC) is one such recently synthesized polycyclic aromatic material,[17] with a structure of a coronene composed of all-sulfur terminated edge framework. It is now well-known as the new generation of sulflower, which upon reduction yields perthiolated coronene (PTC), as shown in Figure 1a. A new two-dimensional
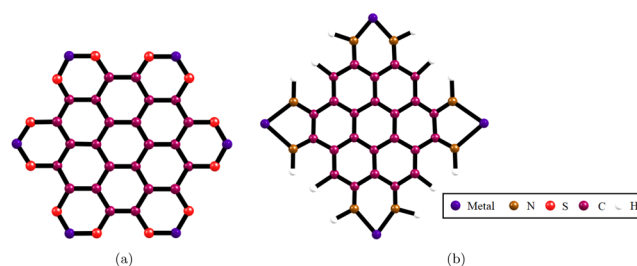
Figure 1. (a) Perthiolated coronene with transition metals. (b) NH-substituted coronene with transition metals.

transition-metal-based conjugated MOF called the black polycrystalline PTC-Fe was synthesized using the PTC framework as an organic ligand unit in conjunction with solvothermal techniques.[18] This MOF is found to exhibit excellent ambient temperature conductivity and is well-suited for electrocatalytic activity, thus finding spintronic applications.[19] Henceforth, a family of such functional MOFs with distinct transition metals like V, Cr, Mn, Fe, Co, and Ni has been made.[20] Subsequently, a 2D-TM-MOF was synthesized with transition metals such as Cr, Mn, Fe, and Co[21] based on an organic unit cell comprising eight −NH-substituted coronene moieties, as depicted in Figure 1b, wherein each −NH moiety is linked to four transition metals establishing a planar geometry. Thus, the study of these newly synthesized and proposed structures can aid in better understanding of their complex structures and functionalities.

Chemical graph theory is a tool that facilitates mathematical characterization of the underlying complex structures of coronene-based MOFs and thus provides insights into their structures and properties. A product of chemical graph theory is the topological index which is a structural descriptor that aids in characterizing the underlying connectivities of complex molecular structures,[22−25] thereby providing tools for the prediction of the properties.[26−31] Furthermore, the International Union of Pure and Applied Chemistry (IUPAC) has also recommended the topological indices for interpreting the descriptions of these MOF crystal structures, as the topology of every MOF structure is unique pertaining to its arrangement of atoms and bonds.[32] A large number of topological indices that are based on topological distances and vertex degrees have been developed over the years in order to predict the physicochemical properties and activities of molecules.[33−42] Likewise, graph entropy based on Shannon's definition is an information−theoretic index that associates deterministic and probabilistic distributions to the topological index functions in order to characterize the underlying structural orders and complexities of molecular structures.[43−45] The entropy-based indices of various molecular frameworks have gained interest in recent years.[46−50] In this study, we obtain the degree and degree-sum-based topological indices and their entropies for three different structures of coronene-based metal organic frameworks which play a significant role in understanding the tunable properties of MOFs and in addressing the complexity of their structural geometries. Furthermore, we employ distance degree vector

sequences together with their symmetry features to obtain the typical NMR and ESR spectroscopic signatures which enable contrast of these structures through potential spectroscopic studies in the future.

2. COMPUTATIONAL METHODS

The coronene-based transition metal organic framework is a simple connected graph in which the accumulation of atoms denotes the vertex set $V(\text{MOF})$ while the bonds are with the edge set $E(\text{MOF})$. In these frameworks, the edges indicate covalent bonds between the atoms while the vertices represent non-hydrogen atoms.

The degree of a vertex $v \in V(\text{MOF})$ denoted by $d_{\text{MOF}}(v)$ is the number of neighboring vertices of v, and the degree-sum of v is the sum of the degree of vertices in the neighborhood of v, denoted as $s_{\text{MOF}}(v)$. That is, $s_{\text{MOF}}(v) = \sum_{w \in N_{\text{MOF}}(v)} d_{\text{MOF}}(w)$ in which we used $N_{\text{MOF}}(v) = \{w \in V(\text{MOF}) | wv \in E(\text{MOF})\}$. Let $d(w,z) = |\{ij \in E(\text{MOF}): d_{\text{MOF}}(i) = w \text{ and } d_{\text{MOF}}(j) = z\}|$ and $s(w,z) = |\{ij \in E(\text{MOF}): s_{\text{MOF}}(i) = w \text{ and } s_{\text{MOF}}(j) = z\}|$. Then the edge set of the MOF can be classified based on the notations $d(w,z)$ and $s(w,z)$, and they are denoted by $D(\text{MOF})$ and $S(\text{MOF})$, respectively.

With respect to the degree and degree-sum classification of MOF, the bond additive and scalar multiplicative molecular descriptor index functions $\{\Psi^d, \Psi^{d*}, \Psi^s, \text{ and } \Psi^{s*}\}$ with specific index representation $\Psi(w,z)$ are defined in the following.

$$\Psi^d(\text{MOF}) = \sum_{d(w,z) \in D(\text{MOF})} d(w,z)\Psi(w,z)$$

$$\Psi^{d^*}(\text{MOF}) = \prod_{d(w,z) \in D(\text{MOF})} d(w,z)\Psi(w,z)$$

$$\Psi^s(\text{MOF}) = \sum_{s(w,z) \in S(\text{MOF})} s(w,z)\Psi(w,z)$$

$$\Psi^{s^*}(\text{MOF}) = \prod_{s(w,z) \in S(\text{MOF})} s(w,z)\Psi(w,z)$$

When we consider the self-powered index functions, the corresponding bond additive and scalar multiplicative descriptors are given as follows:

$$\Psi^{dp}(\text{MOF}) = \sum_{d(w,z) \in D(\text{MOF})} d(w,z)\Psi(w,z)^{\Psi(w,z)}, \quad \Psi^{dp*}(\text{MOF}) = \prod_{d(w,z) \in D(\text{MOF})} d(w,z)\Psi(w,z)^{\Psi(w,z)}$$

$$\Psi^{sp}(\text{MOF}) = \sum_{s(w,z) \in S(\text{MOF})} s(w,z)\Psi(w,z)^{\Psi(w,z)}, \quad \Psi^{sp*}(\text{MOF}) = \prod_{s(w,z) \in S(\text{MOF})} s(w,z)\Psi(w,z)^{\Psi(w,z)}$$

The specific index function $\Psi(w,z)$ for well-known descriptors is given below.[31,49,50]

    (i) First Zagreb index $M_1(w,z) = w + z$
    (ii) Second Zagreb index $M_2(w,z) = wz$
    (iii) Augmented Zagreb index $AZ(w,z) = \left(\frac{wz}{w+z-2}\right)^3$
    (iv) Third redefined Zagreb index $ReZ_3(w,z) = wz(w + z)$
    (v) Hyper Zagreb index $HM(w,z) = (w + z)^2$

    (vi) Atom bond connectivity index $ABC(w,z) = \sqrt{\frac{w+z-2}{wz}}$
    (vii) Geometric−arithmetic index $GA(w,z) = \frac{2\sqrt{wz}}{w+z}$
    (viii) Randić index $R(w,z) = \frac{1}{\sqrt{wz}}$
    (ix) Reduced reciprocal Randić index $RRR(w,z) = \sqrt{(w-1)(z-1)}$
    (x) Inverse sum indeg index $ISI(w,z) = \frac{wz}{w+z}$

(xi) Forgotten index $F(w,z) = w^2 + z^2$

(xii) Harmonic index $H(w,z) = \frac{2}{w+z}$

(xiii) Symmetric degree division index $SDD(w,z) = \left(\frac{w}{z} + \frac{z}{w} \right)$

(xiv) Sombor index $SO(w,z) = \sqrt{w^2 + z^2}$

(xv) Sum connectivity index $SC(w,z) = \frac{1}{\sqrt{w+z}}$

The edge classification notations $d(w,z)$ and $s(w,z)$ just categorize the number of edges with an equal number of atoms at the end vertices, but they do not count the types of atoms, as MOFs have four types of atoms. Hence, we employ the weight function to differentiate the type of atoms as well as for bonds to enhance the bond additive/multiplicative descriptors. The weight function for an atom A is denoted by Φ_A, and bond A−B has a weight function of Γ_{AB}. Consequently, the edge classification of MOFs will be fine-tuned further based on the bond weight function, and the computations of topological descriptors involve the bond weight along with the notations $d(w,z)$ and $s(w,z)$.

To implement Shannon's entropy approach,[51] we define the structural information function f on the edge set of MOF into a non-negative real number, and in our study, the structural information is taken as the bond measure induced from degree/degree-sum parameters. The entropy of MOF structures with structural information f is defined below, assuming that $E(MOF) = \{a_1, a_2, ..., a_n\}$.

$$I_f(MOF) = -\sum_{c=1}^{n} \frac{f(a_c)}{\sum_{g=1}^{n} f(a_g)} \log \left(\frac{f(a_c)}{\sum_{g=1}^{n} f(a_g)} \right)$$

$$= \log \left(\sum_{c=1}^{n} f(a_c) \right) - \frac{1}{\sum_{c=1}^{n} f(a_c)} \log \left(\prod_{c=1}^{n} f(a_c)^{f(a_c)} \right) \quad (1)$$

As discussed in a series of papers,[28,30,45,46] we replace the multiplicative component of the above equation with scalar multiplicative, and we arrive at the modified form of entropy as given below.

$$I_f(MOF) = \log(f(MOF)) - \frac{1}{f(MOF)} \log(f^{p*}(MOF))$$

## 3. RESULTS AND DISCUSSION

The metal organic frameworks with coronene-based organic ligands as anchors and varied transition metals are found to exhibit potential attributes, and the synthesis and proposal techniques of such frameworks have thus attracted the recent interest of theoretical chemists.[18,20,21] We consider three MOFs with two types of unit cells as (i) perthiolated coronene with transition metals placed at the sulfur-terminated edges and (ii) NH-substituted coronene covalently linked to transition metals. Based on the geometry of the arrangement of unit cells, we categorize three MOFs, namely, hexagonal PTC-TM (PTC-TM-H(q)), parallelogram PTC-TM (PTC-TM-P(q,r)), and rectangular NHC-TM (NH-C-TM-R(m,n)) frameworks.

The PTC-TM-H(q) MOF of dimension q is constructed by circumscribing the PTC-TM unit cell with a radius q, as shown in Figure 2, while the PTC-TM-P(q,r) MOF is obtained by arranging the PTC-TM unit cell in a $q \times r$ gridlike pattern, as given in Figure 3. Similarly, NHC-TM-R(m,n) is derived by the rectangular arrangement of the NHC-TM unit cell in the $m \times n$ grid design, as depicted in Figure 4.
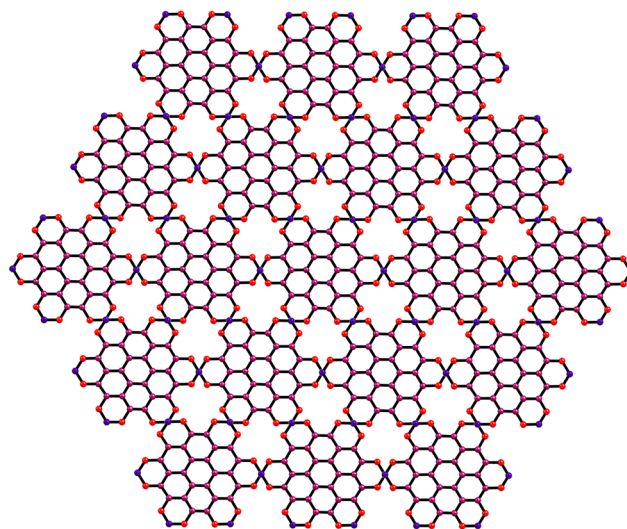
Figure 2. Stacking of perthiolated coronene in a hexagonal shape with dimension 3.
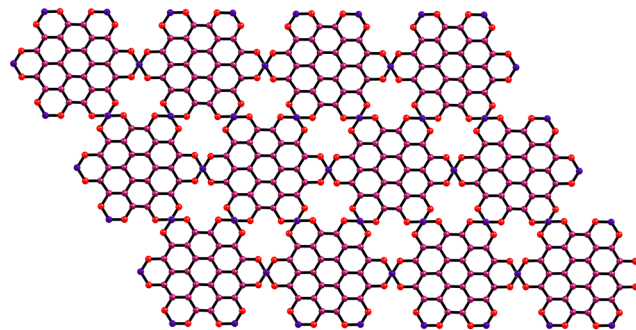
Figure 3. Stacking of perthiolated coronene in a parallelogram shape with dimensions (3,4).
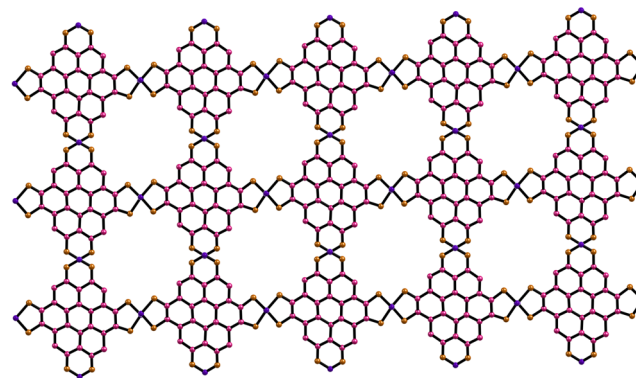
Figure 4. Stacking of NH-substituted coronene in a rectangular shape with dimensions (3,5).

The MOF PTC-TM-H(q) contains $117q^2 - 111q + 36$ number of vertices and $162q^2 - 162q + 54$ number of edges, whereas PTC-TM-P(q,r) contains $39qr + 2q + 2r - 1$ number of vertices and $54qr$ number of edges. Similarly, the number of vertices and edges of NH-C-TM-R(m,n) are $34mn + m + n$ and $46mn$, respectively. We now present the topological characterization of the discussed MOFs in the following. Further, the topological expressions were validated with TopoChemie-2020[52] software, and all the computed results from the codes agree with those obtained from the analytical expressions.

Table 1. Classification of Degree Bond Partition for PTC-TM

		MOF, with its frequency	
bond A−B	$(d_{MOF}(A), d_{MOF}(B))$	PTC-TM-H(q)	PTC-TM-P(q,r)
M−S	$(2\Phi_S, \Phi_M + \Phi_C)$	$24q - 12$	$8q + 8r - 4$
	$(4\Phi_S, \Phi_C + \Phi_M)$	$36q^2 - 60q + 24$	$12qr - 8q - 8r + 4$
S−C	$(\Phi_M + \Phi_C, 2\Phi_C + \Phi_S)$	$36q^2 - 36q + 12$	$12qr$
	$(3\Phi_C, 3\Phi_C)$	$36q^2 - 36q + 12$	$12qr$
C−C	$(\Phi_S + 2\Phi_C, 3\Phi_C)$	$36q^2 - 36q + 12$	$12qr$
	$(\Phi_S + 2\Phi_C, \Phi_S + 2\Phi_C)$	$18q^2 - 18q + 6$	$6qr$

Table 2. Classification of Degree-Sum Bond Partition for PTC-TM

		MOF, with its frequency	
bond A−B	$(s_{MOF}(A), s_{MOF}(B))$	PTC-TM-H(q)	PTC-TM-P(q,r)
M−S	$(4\Phi_S, 2\Phi_M + 3\Phi_C)$	$24q - 12$	$8q + 8r - 4$
	$(8\Phi_S, 3\Phi_C + 4\Phi_M)$	$36q^2 - 60q + 24$	$12qr - 8q - 8r + 4$
S−C	$(2\Phi_M + 3\Phi_C, 6\Phi_C + 2\Phi_S)$	$24q - 12$	$8q + 8r - 4$
	$(4\Phi_M + 3\Phi_C, 6\Phi_C + 2\Phi_S)$	$36q^2 - 60q + 24$	$12qr - 8q - 8r + 4$
	$(9\Phi_C, 9\Phi_C)$	$36q^2 - 36q + 12$	$12qr$
C−C	$(2\Phi_S + 6\Phi_C, 9\Phi_C)$	$36q^2 - 36q + 12$	$12qr$
	$(2\Phi_S + 6\Phi_C, 2\Phi_S + 6\Phi_C)$	$18q^2 - 18q + 6$	$6qr$

3.1. Degree and Degree-Sum-Based Molecular Descriptors.

The different bond additive degree and degree-sum-based molecular descriptors of crystalline MOFs, where the MOF takes hexagonal PTC-TM-H(q) for $q \geq 1$, parallelogram PTC-TM-P(q,r) for $(q,r) \geq 1$, and rectangular NHC-TM-R(m,n) for $(m,n) \geq 1$, are evaluated on the basis of bond distributions presented in Tables 1−4, in which $\Psi \in \{M_1, M_2, ReZ_3, HM, AZ, R, RRR, SC, ISI, F, H, ABC, GA, SO, SDD\}$.

For the index function Ψ, the degree descriptors of PTC-TM-H(q) are derived by the equation

$$\Psi^d(\text{PTC-TM-H}(q)) = (24q - 12)\Gamma_{MS}\Psi(2\Phi_S, \Phi_C + \Phi_M)$$
$$+ (36q^2 - 60q + 24)\Gamma_{MS}\Psi(4\Phi_S, \Phi_C + \Phi_M)$$
$$+ (36q^2 - 36q + 12)\Gamma_{SC}\Psi(\Phi_M + \Phi_C, 2\Phi_C + \Phi_S)$$
$$+ (36q^2 - 36q + 12)\Gamma_{CC}\Psi_{(3\Phi_C, 3\Phi_C)}$$
$$+ (36q^2 - 36q + 12)\Gamma_{CC}\Psi(\Phi_S + 2\Phi_C, 3\Phi_C)$$
$$+ (18q^2 - 18q + 6)\Gamma_{CC}\Psi(\Phi_S + 2\Phi_C, \Phi_S + 2\Phi_C)$$

and the degree-sum descriptors of PTC-TM-H(q) are obtained by the equation

$$\Psi^s(\text{PTC-TM-H}(q)) = (24q - 12)\Gamma_{MS}\Psi(4\Phi_S, 2\Phi_M + 3\Phi_C)$$
$$+ (36q^2 - 60q + 24)\Gamma_{MS}\Psi(8\Phi_S, 3\Phi_C + 4\Phi_M)$$
$$+ (24q - 12)\Gamma_{SC}\Psi(2\Phi_M + 3\Phi_C, 6\Phi_C + 2\Phi_S)$$
$$+ (36q^2 - 60q + 24)\Gamma_{SC}\Psi(4\Phi_M + 3\Phi_C, 6\Phi_C + 2\Phi_S)$$
$$+ (36q^2 - 36q + 12)\Gamma_{CC}\Psi(2\Phi_S + 6\Phi_C, 9\Phi_C)$$
$$+ (18q^2 - 18q + 6)\Gamma_{CC}\Psi(2\Phi_S + 6\Phi_C, 2\Phi_S + 6\Phi_C)$$
$$+ (36q^2 - 36q + 12)\Gamma_{CC}\Psi(9\Phi_C, 9\Phi_C)$$

To derive the quantitative expressions of topological descriptors for PTC-TM-H(q), we set the atom and bond weights by unity, and produce the following the result. In the sequel, $\# \in \{d,s\}$, we write $\Psi^\#$ (MOF) to represent $\{\Psi^d(\text{MOF}), \Psi^s(\text{MOF})\}$.

Table 3. Classification of Degree Bond Partition for NHC-TM

		MOF, with its frequency
bond A−B	$(d_{MOF}(A), d_{MOF}(B))$	NHC-TM-R(m,n)
M−N	$(2\Phi_N, \Phi_M + \Phi_C)$	$4m + 4n$
	$(4\Phi_N, \Phi_M + \Phi_C)$	$8mn - 4m - 4n$
N−C	$(\Phi_M + \Phi_C, 2\Phi_C + \Phi_N)$	$8mn$
	$(3\Phi_C, 3\Phi_C)$	$12mn$
	$(2\Phi_C, 3\Phi_C)$	$4mn$
C−C	$(\Phi_N + 2\Phi_C, 2\Phi_C)$	$4mn$
	$(2\Phi_C + \Phi_N, 3\Phi_C)$	$8mn$
	$(2\Phi_C + \Phi_N, 2\Phi_C + \Phi_N)$	$2mn$
N−H		$8mn$
C−H		$4mn$

Table 4. Classification of Degree-Sum Bond Partition for NHC-TM

		MOF, with its frequency
bond A−B	$(s_{MOF}(A), s_{MOF}(B))$	NHC-TM-R(m,n)
M−N	$(4\Phi_N, 2\Phi_M + 3\Phi_C)$	$4m + 4n$
	$(8\Phi_N, 4\Phi_M + 3\Phi_C)$	$8mn - 4m - 4n$
N−C	$(2\Phi_M + 3\Phi_C, 5\Phi_C + 2\Phi_N)$	$4n$
	$(2\Phi_M + 3\Phi_C, 6\Phi_C + 2\Phi_N)$	$4m$
	$(4\Phi_M + 3\Phi_C, 6\Phi_C + 2\Phi_N)$	$4nm - 4n$
	$(4\Phi_M + 3\Phi_C, 5\Phi_C + 2\Phi_N)$	$4mn - 4m$
	$(9\Phi_C, 9\Phi_C)$	$8mn$
	$(2\Phi_N + 5\Phi_C, 6\Phi_C)$	$4mn$
	$(2\Phi_N + 5\Phi_C, 9\Phi_C)$	$4mn$
C−C	$(6\Phi_C + 2\Phi_N, 6\Phi_C + 2\Phi_N)$	$2mn$
	$(6\Phi_C, 8\Phi_C)$	$4mn$
	$(8\Phi_C, 9\Phi_C)$	$4mn$
	$(8\Phi_C, 2\Phi_N + 6\Phi_C)$	$4mn$

Result 1. *The molecular descriptors of transition metal organic frameworks* PTC-TM-H *with size q are given by*
1. $M_1^\#(\text{PTC-TM-H}(q)) = \{936q^2 - 984q + 336, 2628q^2 - 2820q + 972\}$
2. $M_2^\#(\text{PTC-TM-H}(q)) = \{1314q^2 - 1410q + 486, 10692q^2 - 11940q + 4188\}$

3. $ABC^{\#}(PTC\text{-}TM\text{-}H(q)) = \{(36\sqrt{2}+60)q^2 - (36\sqrt{2}+60)q$
$+ (12\sqrt{2}+20),$
$((945\sqrt{14}+1260\sqrt{30}+1080\sqrt{182}+6720)q^2$
$+ (1008\sqrt{35}+504\sqrt{110}-1800\sqrt{182}$
$- 945\sqrt{14}-1260\sqrt{30}-6720)q + (315\sqrt{14}-504\sqrt{35}-252\sqrt{110}$
$+ 420\sqrt{30}+720\sqrt{182}+2240))/420\}$

4. $R^{\#}(PTC\text{-}TM\text{-}H(q)) = \{(6\sqrt{6}+9\sqrt{2}+30)q^2$
$- \quad (6\sqrt{6}+15\sqrt{2}+18)q + (2\sqrt{6}+6\sqrt{2}+4),$
$((1260\sqrt{2}+1080\sqrt{14}+2625)q^2 +$
$(1008\sqrt{5}+504\sqrt{10}-1800\sqrt{14}-1260\sqrt{2}-2625)q$
$+ (720\sqrt{14}-252\sqrt{10}-504\sqrt{5}+420\sqrt{2}+875))/420\}$

5. $GA^{\#}(PTC\text{-}TM\text{-}H(q)) = \{((450+120\sqrt{2}+72\sqrt{6})q^2$
$- (330+200\sqrt{2}+72\sqrt{6})q + 24\sqrt{6}+80\sqrt{2}+90)/5,$
$((179010+84240\sqrt{2}+63648\sqrt{14})q^2 + (-179010-84240\sqrt{2}$
$+ 35360\sqrt{5}+24480\sqrt{10}-106080\sqrt{14})q$
$+ (59670+28080\sqrt{2}-17680\sqrt{5}-12240\sqrt{10}+42432\sqrt{14}))$
$/3315\}$

6. $AZ^{\#}(PTC\text{-}TM\text{-}H(q)) = \{(51237q^2 - 51237q + 17079)/$
$32, \quad (8095195192535734025316321q^2 - 9160897297052204882494071q + 3231249449770146770360982)/$
$50196334196346060800\}$

7. $ReZ_3^{\#}(PTC\text{-}TM\text{-}H(q)) = \{7668q^2 - 8436q + 2940,$
$175464q^2 - 198984q + 70248\}$

8. $SC^{\#}(PTC\text{-}TM\text{-}H(q)) = \{((105\sqrt{6}+36\sqrt{5})q^2$
$- (125\sqrt{6}+36\sqrt{5}-60)q + (45\sqrt{6}+12\sqrt{5}-30))/5,$
$((13260\sqrt{2}+10608\sqrt{15}+4680\sqrt{17}+9945)q^2$
$+ (4080\sqrt{13}-17680\sqrt{15}-4680\sqrt{17}-13260\sqrt{2}+7735)q$
$+ (4420\sqrt{2}+1560\sqrt{17}+7072\sqrt{15}-2040\sqrt{13}-5525))/2210\}$

9. $RRR^{\#}(PTC\text{-}TM\text{-}H(q)) = \{(36\sqrt{3}+36\sqrt{2}+180)q^2 - (60\sqrt{3}+36\sqrt{2}+156)q + (24\sqrt{3}+12\sqrt{2}+48), (72\sqrt{14} + 72\sqrt{42}+414)q^2 + 48\sqrt{3}+ (48\sqrt{7}-72\sqrt{14}-120\sqrt{42} - 414)q + (48\sqrt{42}+24\sqrt{14}-24\sqrt{7}-24\sqrt{3}+138)\}$

10. $ISI^{\#}(PTC\text{-}TM\text{-}H(q)) = \{(1131q^2 - 1171q + 397)/5, (2172222q^2 - 2344670q + 810298)/3315\}$

11. $F^{\#}(PTC\text{-}TM\text{-}H(q)) = \{2808q^2 - 3096q + 1080, 21168q^2 - 23472q + 8208\}$

12. $H^{\#}(PTC\text{-}TM\text{-}H(q)) = \{(282q^2 - 262q + 84)/5, (266331 q^2 - 231515q + 71369)/13260\}$

13. $SDD^{\#}(PTC\text{-}TM\text{-}H(q)) = \{348q^2 - 360q + 122, (68415 q^2 - 67209q + 22202)/210\}$

14. $SO^{\#}(PTC\text{-}TM\text{-}H(q)) = \{(36\sqrt{13}+72\sqrt{5}$
$+ 270\sqrt{2})q^2 - (36\sqrt{13}+120\sqrt{5}+222\sqrt{2})q$
$+ (12\sqrt{13}+48\sqrt{5}+66\sqrt{2}), (468\sqrt{2}+72\sqrt{113}$
$+ 36\sqrt{145})q^2 + (24\sqrt{41}$
$- 468\sqrt{2}+24\sqrt{89}-120\sqrt{113}-36\sqrt{145})q$
$+ (12\sqrt{145}+48\sqrt{113}-12\sqrt{89}-12\sqrt{41}+156\sqrt{2})\}$

15. $HM^{\#}(PTC\text{-}TM\text{-}H(q)) = \{5436q^2 - 5916q + 2052, 42876q^2 - 47676q + 16692\}$

The topological degree/degree-sum molecular descriptors pertaining to PTC-TM-P(q,r) are generated through the following equations:

$$\Psi^d(PTC\text{-}TM\text{-}P(q,r)) = (8q+8r-4)\Gamma_{MS}\Psi(2\Phi_S,\Phi_C+\Phi_M) + (12qr-8q-8r+4)\Gamma_{MS}\Psi(4\Phi_S,\Phi_C+\Phi_M)$$
$$+ (12qr)\Gamma_{SC}\Psi(\Phi_M+\Phi_C,2\Phi_C+\Phi_S) + (12qr)\Gamma_{CC}\Psi(3\Phi_C,3\Phi_C) + (12qr)\Gamma_{CC}\Psi(\Phi_S+2\Phi_C,3\Phi_C) + (6qr)\Gamma_{CC}\Psi(\Phi_S+2\Phi_C,\Phi_S+2\Phi_C)$$

$$\Psi^s(PTC\text{-}TM\text{-}P(q,r)) = (8q+8r-4)\Gamma_{MS}\Psi(4\Phi_S,2\Phi_M+3\Phi_C) + (12qr-8q-8r+4)\Gamma_{MS}\Psi(8\Phi_S,3\Phi_C+4\Phi_M)$$
$$+ (8q+8r-4)\Gamma_{SC}\Psi(2\Phi_M+3\Phi_C,6\Phi_C+2\Phi_S) + (12qr-8q-8r+4)\Gamma_{SC}\Psi(4\Phi_M+3\Phi_C,6\Phi_C+2\Phi_S) + \Gamma_{CC}(12qr)\Psi(9\Phi_C,9\Phi_C)$$
$$+ \Gamma_{CC}(12qr)\Psi(2\Phi_S+6\Phi_C,9\Phi_C) + \Gamma_{CC}(6qr)\Psi(2\Phi_S+6\Phi_C,2\Phi_S+6\Phi_C)$$

The above two equations are simplified by replacing the unit weight for atoms and bonds, we derive the following result.

Result 2. *The molecular descriptors of transition metal organic frameworks PTC-TM-P with size (q,r) are given by*

1. $M_1^{\#}(PTC\text{-}TM\text{-}P(q,r)) = \{312qr - 16q - 16r + 8, 876qr - 64q - 64r + 32\}$

2. $M_2^{\#}(PTC\text{-}TM\text{-}P(q,r)) = \{438qr - 32q - 32r + 16, 3564qr - 416q - 416r + 208\}$

3. $ABC^{\#}(PTC\text{-}TM\text{-}P(q,r)) = \{(20+12\sqrt{2})qr, (120\sqrt{182}-168\sqrt{35}$
$- 84\sqrt{110}+(2240+315\sqrt{14}+420\sqrt{30}+360\sqrt{182})qr$
$+ (336\sqrt{35}+168\sqrt{110}-240\sqrt{182})q + (336\sqrt{35}+168\sqrt{110}$
$- 240\sqrt{182})r)/420\}$

4. $R^{\#}(PTC\text{-}TM\text{-}P(q,r)) = \{(2\sqrt{6}+3\sqrt{2}+10)qr + (4-2\sqrt{2})q$
$+ (4-2\sqrt{2})r + (\sqrt{2}-2), ((360\sqrt{14}+420\sqrt{2}+875)qr$
$+ (168\sqrt{10}+336\sqrt{5}-240\sqrt{14})q + (168\sqrt{10}+336\sqrt{5}-240\sqrt{14})r$
$+ (120\sqrt{14}-84\sqrt{10}-168\sqrt{5}))/420\}$

5. $GA^{\#}(PTC\text{-}TM\text{-}P(q,r)) = \{((72\sqrt{6}+120\sqrt{2}+450)qr + (120-80\sqrt{2})q$
$+ (120-80\sqrt{2})r + 40\sqrt{2}-60)/15,$
$((63648\sqrt{14}+84240\sqrt{2}+179010)qr + (24480\sqrt{10}-42432\sqrt{14}$
$+ 35360\sqrt{5})q + (24480\sqrt{10}+35360\sqrt{5}-42432\sqrt{14})r$
$+ (21216\sqrt{14}-12240\sqrt{10}-17680\sqrt{5}))/9945\}$

6. $AZ^{\#}(PTC\text{-}TM\text{-}P(q,r)) = \{17079qr/32, (269839839751\text{-}1911341772107qr - 355234034838823619059250q - 355234034838823619059250r + 1776170174194118095 29625)/50196334196346060800\}$

7. $ReZ_3^{\#}(PTC\text{-}TM\text{-}P(q,r)) = \{2556qr - 256q256r + 128, 58488qr - 7840q - 7840r + 3920\}$

8. $SC^{\#}(PTC\text{-}TM\text{-}P(q,r)) = \{((36\sqrt{5}+105\sqrt{6})qr$
$+ (60-20\sqrt{6})q + (60-20\sqrt{6})r + (10\sqrt{6}-30))$
$/15, ((4680\sqrt{17}+10608\sqrt{15}+13260\sqrt{2}+9945)qr$
$+ (4080\sqrt{13}-7072\sqrt{15}+17680)q + (4080\sqrt{13}-7072\sqrt{15}+17680)r$
$+ (3536\sqrt{15}-2040\sqrt{13}-8840))/6630\}$

Table 5. Entropy Values Induced from Degree and Degree-Sum Descriptors for PTC-TM-H(q)

	f	$q = 2$	$q = 3$	$q = 4$	$q = 5$	$q = 6$	$q = 7$	$q = 8$	$q = 9$	$q = 10$
M_1	d	7.631	8.657	9.334	9.839	10.242	10.578	10.865	11.116	11.339
	s	8.628	9.674	10.357	10.865	11.269	11.606	11.894	12.145	12.369
M_2	d	7.956	8.988	9.667	10.174	10.578	10.914	11.201	11.453	11.676
	s	9.986	11.054	11.745	12.256	12.664	13.002	13.291	13.543	13.767
ABC	d	5.493	6.526	7.205	7.710	8.113	8.449	8.736	8.986	9.209
	s	5.080	6.133	6.818	7.326	7.730	8.066	8.353	8.604	8.827
R	d	4.823	5.868	6.550	7.056	7.459	7.795	8.082	8.332	8.555
	s	3.489	4.692	5.430	5.963	6.381	6.724	7.017	7.271	7.497
GA	d	5.877	6.898	7.573	8.077	8.479	8.813	9.100	9.350	9.573
	s	5.866	6.902	7.581	8.087	8.490	8.825	9.113	9.363	9.586
AZ	d	8.200	9.215	9.886	10.388	10.789	11.123	11.409	11.659	11.881
	s	10.383	11.457	12.151	12.664	13.072	13.410	13.699	13.952	14.176
ReZ_3	d	9.692	10.738	11.422	11.931	12.336	12.673	12.961	13.213	13.437
	s	12.735	13.832	14.531	15.047	15.456	15.795	16.085	16.338	16.562
SC	d	4.983	6.026	6.708	7.215	7.619	7.954	8.241	8.492	8.715
	s	4.351	5.459	6.163	6.681	7.090	7.429	7.718	7.971	8.195
RRR	d	6.459	7.490	8.169	8.675	9.079	9.415	9.702	9.954	10.177
	s	7.799	8.844	9.527	10.036	10.441	10.777	11.065	11.317	11.541
ISI	d	6.210	7.238	7.915	8.420	8.823	9.159	9.446	9.697	9.920
	s	7.244	8.285	8.967	9.475	9.879	10.216	10.504	10.756	10.979
F	d	8.690	9.734	10.418	10.926	11.331	11.668	11.957	12.208	12.432
	s	10.681	11.753	12.432	12.956	13.363	13.701	13.990	14.242	14.466
H	d	4.810	5.853	6.534	7.040	7.443	7.778	8.065	8.315	8.538
	s	3.482	4.687	5.427	5.960	6.378	6.722	7.015	7.269	7.495
SDD	d	6.647	7.672	8.348	8.852	9.255	9.590	9.877	10.128	10.351
	s	6.602	7.621	8.293	8.796	9.197	9.531	9.817	10.067	10.290
SO	d	7.295	8.324	9.001	9.507	9.910	10.246	10.533	10.785	11.008
	s	8.289	9.331	10.013	10.521	10.925	11.261	11.549	11.800	12.024
HM	d	9.356	10.399	11.082	11.590	11.994	12.331	12.619	12.871	13.094
	s	11.359	12.438	13.118	13.645	14.051	14.390	14.679	14.932	15.156

9. $\mathrm{RRR}^{\#}(\text{PTC-TM-P}(q,r)) = \{12(5 + \sqrt{2} + \sqrt{3})qr + 8(1 - \sqrt{3})q$
$+ 8(1 - \sqrt{3})r + 4(\sqrt{3} - 1),$
$(24\sqrt{42} + 24\sqrt{14} + 138)qr + (16\sqrt{7} + 16\sqrt{3} - 16\sqrt{42})q$
$+ (16\sqrt{7} + 16\sqrt{3} - 16\sqrt{42})r + (8\sqrt{42} - 8\sqrt{7} - 8\sqrt{3})\}$

10. $\mathrm{ISI}^{\#}(\text{PTC-TM-P}(q,r)) = \{(1131qr - 40q - 40r + 20)/15,$
$(2172222qr - 172448q - 172448r + 86224)/9945\}$

11. $\mathrm{F}^{\#}(\text{PTC-TM-P}(q,r)) = \{936qr - 96q - 96r + 48, 7164qr$
$- 768q - 768r + 384\}$

12. $\mathrm{H}^{\#}(\text{PTC-TM-P}(q,r)) = \{(282qr + 20q + 20r - 10)/15,$
$(266331qr + 34816q + 34816r - 17408)/39780\}$

13. $\mathrm{SDD}^{\#}(\text{PTC-TM-P}(q,r)) = \{(116qr - 4q - 4r + 2,$
$22805qr + 402q + 402r - 201)/210\}$

14. $\mathrm{SO}^{\#}(\text{PTC-TM-P}(q,r)) = \{(12\sqrt{13} + 24\sqrt{5} + 90\sqrt{2})qr$
$+ (16\sqrt{2} - 16\sqrt{5})q + (16\sqrt{2} - 16\sqrt{5})r + (8\sqrt{5} - 8\sqrt{2}),$
$(12\sqrt{145} + 24\sqrt{113} + 156\sqrt{2})qr + (8\sqrt{89} + 8\sqrt{41} - 16\sqrt{113})q$
$+ (8\sqrt{89} + 8\sqrt{41} - 16\sqrt{113})r + (8\sqrt{113} - 4\sqrt{89} - 4\sqrt{41})\}$

15. $\mathrm{HM}^{\#}(\text{PTC-TM-P}(q,r)) = \{1812qr - 160q - 160r + 80,$
$14292qr - 1600q - 1600r + 800\}$

To derive the molecular descriptors of NHC-TM-R(m,n), we use the bond classification from Tables 3 and 4 and in line with the following equations.

$$\Psi^d(\text{NHC-TM-R}(m,n)) = (4m + 4n)\Gamma_{\mathrm{MN}}\Psi(2\Phi_{\mathrm{N}}, \Phi_{\mathrm{M}} + \Phi_{\mathrm{C}}) + \Gamma_{\mathrm{MN}}(8mn - 4m - 4n)\Psi(4\Phi_{\mathrm{N}}, \Phi_{\mathrm{M}} + \Phi_{\mathrm{C}})$$
$$+ (8mn)\Gamma_{\mathrm{NC}}\Psi(\Phi_{\mathrm{M}} + \Phi_{\mathrm{C}}, 2\Phi_{\mathrm{C}} + \Phi_{\mathrm{N}}) + (4mn)\Gamma_{\mathrm{NC}}\Psi(2\Phi_{\mathrm{C}} + \Phi_{\mathrm{N}}, 2\Phi_{\mathrm{C}}) + (12mn)\Gamma_{\mathrm{CC}}\Psi(3\Phi_{\mathrm{C}}, 3\Phi_{\mathrm{C}}) + (4mn)\Gamma_{\mathrm{CC}}\Psi(2\Phi_{\mathrm{C}}, 3\Phi_{\mathrm{C}})$$
$$+ (8mn)\Gamma_{\mathrm{CC}}\Psi(2\Phi_{\mathrm{C}} + \Phi_{\mathrm{N}}, 3\Phi_{\mathrm{C}}) + (2mn)\Gamma_{\mathrm{CC}}\Psi(2\Phi_{\mathrm{C}} + \Phi_{\mathrm{N}}, 2\Phi_{\mathrm{C}} + \Phi_{\mathrm{N}})$$

$$\Psi^s(\text{NHC-TM-R}(m,n)) = (4m + 4n)\Gamma_{\mathrm{MN}}\Psi(4\Phi_{\mathrm{N}}, 2\Phi_{\mathrm{M}} + 3\Phi_{\mathrm{C}})) + (8mn - 4m - 4n)\Gamma_{\mathrm{MN}}\Psi(8\Phi_{\mathrm{N}}, 4\Phi_{\mathrm{M}} + 3\Phi_{\mathrm{C}})$$
$$+ (4m)\Gamma_{\mathrm{NC}}\Psi(2\Phi_{\mathrm{M}} + 3\Phi_{\mathrm{C}}, 6\Phi_{\mathrm{C}} + 2\Phi_{\mathrm{N}}) + (4nm - 4n)\Gamma_{\mathrm{NC}}\Psi(4\Phi_{\mathrm{M}} + 3\Phi_{\mathrm{C}}, 6\Phi_{\mathrm{C}} + 2\Phi_{\mathrm{N}})$$
$$+ (4n)\Gamma_{\mathrm{NC}}\Psi(2\Phi_{\mathrm{M}} + 3\Phi_{\mathrm{C}}, 5\Phi_{\mathrm{C}} + 2\Phi_{\mathrm{N}}) + (4mn - 4m)\Gamma_{\mathrm{NC}}\Psi(4\Phi_{\mathrm{M}} + 3\Phi_{\mathrm{C}}, 5\Phi_{\mathrm{C}} + 2\Phi_{\mathrm{N}}) + (8mn)\Gamma_{\mathrm{CC}}\Psi(9\Phi_{\mathrm{C}}, 9\Phi_{\mathrm{C}})$$
$$+ (2mn)\Gamma_{\mathrm{CC}}\Psi(2\Phi_{\mathrm{N}} + 6\Phi_{\mathrm{C}}, 2\Phi_{\mathrm{N}} + 6\Phi_{\mathrm{C}}) + (4mn)\Gamma_{\mathrm{CC}}\Psi(8\Phi_{\mathrm{C}}, 9\Phi_{\mathrm{C}}) + (4mn)\Gamma_{\mathrm{CC}}\Psi(2\Phi_{\mathrm{N}} + 5\Phi_{\mathrm{C}}, 9\Phi_{\mathrm{C}})$$
$$+ (4mn)\Gamma_{\mathrm{CC}}\Psi(2\Phi_{\mathrm{N}} + 5\Phi_{\mathrm{C}}, 6\Phi_{\mathrm{C}}) + (4mn)\Gamma_{\mathrm{CC}}\Psi(6\Phi_{\mathrm{C}}, 8\Phi_{\mathrm{C}}) + (4mn)\Gamma_{\mathrm{CC}}\Psi(8\Phi_{\mathrm{C}}, 2\Phi_{\mathrm{N}} + 6\Phi_{\mathrm{C}})$$

Table 6. Entropy Values Induced from Degree and Degree-Sum Descriptors for PTC-TM-P(q,q)

	f	$q = 2$	$q = 3$	$q = 4$	$q = 5$	$q = 6$	$q = 7$	$q = 8$	$q = 9$	$q = 10$
M_1	d	7.041	7.889	8.480	8.935	9.305	9.617	9.886	10.124	10.336
	s	8.017	8.892	9.493	9.953	10.327	10.640	10.911	11.150	11.363
M_2	d	7.361	8.215	8.809	9.266	9.637	9.950	10.220	10.459	10.671
	s	9.349	10.255	10.869	11.336	11.713	12.030	12.303	12.543	12.757
ABC	d	4.902	5.756	6.350	6.806	7.177	7.489	7.759	7.996	8.208
	s	4.471	5.351	5.956	6.418	6.791	7.105	7.376	7.614	7.826
R	d	4.223	5.092	5.693	6.152	6.524	6.836	7.106	7.344	7.556
	s	2.748	3.811	4.499	5.005	5.404	5.735	6.017	6.263	6.481
GA	d	5.296	6.136	6.724	7.177	7.546	7.856	8.125	8.362	8.573
	s	5.271	6.129	6.725	7.182	7.553	7.865	8.135	8.373	8.585
AZ	d	7.629	8.457	9.041	9.491	9.858	10.168	10.436	10.672	10.883
	s	9.737	10.653	11.271	11.740	12.118	12.436	12.709	12.950	13.165
ReZ_3	d	9.081	9.954	10.556	11.017	11.391	11.705	11.977	12.216	12.429
	s	12.062	13.013	13.643	14.117	14.498	14.818	15.092	15.334	15.549
SC	d	4.382	5.250	5.850	6.309	6.681	6.994	7.264	7.502	7.714
	s	3.692	4.640	5.275	5.753	6.136	6.456	6.731	6.973	7.187
RRR	d	5.867	6.718	7.311	7.768	8.139	8.452	8.722	8.960	9.173
	s	7.190	8.062	8.663	9.123	9.496	9.811	10.082	10.321	10.534
ISI	d	5.622	6.469	7.061	7.516	7.886	8.198	8.468	8.705	8.917
	s	6.639	7.505	8.104	8.563	8.936	9.250	9.521	9.760	9.973
F	d	8.082	8.951	9.552	10.013	10.386	10.701	10.972	11.211	11.425
	s	10.039	10.952	11.568	12.035	12.412	12.729	13.002	13.242	13.456
H	d	4.211	5.079	5.678	6.137	6.508	6.821	7.090	7.327	7.539
	s	2.738	3.805	4.494	5.001	5.401	5.731	6.014	6.260	6.478
SDD	d	6.061	6.905	7.495	7.949	8.319	8.630	8.900	9.137	9.349
	s	6.021	6.861	7.447	7.899	8.266	8.576	8.844	9.081	9.292
SO	d	6.705	7.554	8.146	8.601	8.972	9.284	9.554	9.792	10.004
	s	7.681	8.551	9.151	9.610	9.983	10.296	10.567	10.806	11.019
HM	d	8.749	9.618	10.218	10.678	11.051	11.365	11.636	11.875	12.088
	s	10.707	11.632	12.252	12.721	13.100	13.417	13.691	13.931	14.145

Result 3. *The molecular descriptors of transition metal organic frameworks NHC-TM-R with size (m,n) are given by*

1. $M_1^{\#}(\text{NHC-TM-R}(m,n)) = \{260mn - 8m - 8n, 716mn - 28m - 36n\}$

2. $M_2^{\#}(\text{NHC-TM-R}(m,n)) = \{358mn - 16m - 16n, 2800mn - 180m - 228n\}$

3. $ABC^{\#}(\text{NHC-TM-R}(m,n)) = \{(44 + 36\sqrt{2})mn / 3,$
   $((7000 + 1680\sqrt{2} + 1440\sqrt{3} + 945\sqrt{14} + 420\sqrt{30} + 540\sqrt{182}$
   $+ 120\sqrt{462})mn + (504\sqrt{35} - 1440\sqrt{3} + 252\sqrt{110} - 180\sqrt{182})m$
   $+ (720\sqrt{14} + 504\sqrt{35} - 360\sqrt{182})n) / 1260\}$

4. $R^{\#}(\text{NHC-TM-R}(m,n)) = \{((22 + 6\sqrt{2} + 8\sqrt{6})mn + (6 - 3\sqrt{2})m$
   $+ (6 - 3\sqrt{2})n) / 3, ((420\sqrt{2} + 420\sqrt{3} + 240\sqrt{7} + 540\sqrt{14}$
   $+ 120\sqrt{42} + 2785)mn + (504\sqrt{5} + 252\sqrt{10} - 180\sqrt{14} - 720)m$
   $+ (504\sqrt{5} - 360\sqrt{14} + 144\sqrt{35})n) / 1260\}$

5. $GA^{\#}(\text{NHC-TM-R}(m,n)) = \{((330 + 80\sqrt{2} + 96\sqrt{6})mn + (60 - 40\sqrt{2})m$
   $+ (60 - 40\sqrt{2})n) / 15,$
   $((393120\sqrt{2} + 318240\sqrt{3} + 208845\sqrt{7} + 445536\sqrt{14} + 85680\sqrt{42}$
   $+ 2506140)mn + (247520\sqrt{5} + 171360\sqrt{10} - 148512\sqrt{14} - 556920)m$
   $+ (247520\sqrt{5} - 297024\sqrt{14} + 92820\sqrt{35})n) / 139230\}$

6. $AZ^{\#}(\text{NHC-TM-R}(m,n)) = \{14163mn / 32, (2072226469123$
   $319478858744mn - 15382286265894025489737 5m$
   $- 188076221284433323257625n) / 501963341963460608000\}$

7. $ReZ_3^{\#}(\text{NHC-TM-R}(m,n)) = \{2052mn - 128m - 128n,$
   $44432mn - 3304m - 4320n\}$

8. $SC^{\#}(\text{NHC-TM-R}(m,n)) = \{((48\sqrt{5} + 75\sqrt{6})mn + (30 - 10\sqrt{6})m$
   $+ (30 - 10\sqrt{6})n) / 15, ((116025 + 37128\sqrt{15} + 61880\sqrt{2} + 14280\sqrt{13}$
   $+ 26520\sqrt{14} + 10920\sqrt{17})mn + (61880 + 14280\sqrt{13} - 13260\sqrt{14}$
   $- 12376\sqrt{15})m + (61880 + 30940\sqrt{3} - 24752\sqrt{15})n) / 46410\}$

9. $RRR^{\#}(\text{NHC-TM-R}(m,n)) = \{(8\sqrt{3} + 16\sqrt{2} + 44)mn + (4 - 4\sqrt{3})m$
   $+ (4 - 4\sqrt{3})n, (12\sqrt{42} + 4\sqrt{35} + 4\sqrt{30} + 8\sqrt{14} + 16\sqrt{3} + 130)mn$
   $+ (8\sqrt{7} + 8\sqrt{3} - 4\sqrt{42} - 24)m + (8\sqrt{6} + 8\sqrt{3} - 8\sqrt{42})n)\}$

10. $ISI^{\#}(\text{NHC-TM-R}(m,n)) = \{943mn - 20m - 20n/15,$
    $(49601673mn - 2154376m - 2592772n)/278460\}$

11. $F^{\#}(\text{NHC-TM-R}(m,n)) = \{764mn - 48m - 48n, 5652mn$
    $- 324m - 444n\}$

12. $H^{\#}(\text{NHC-TM-R}(m,n)) = \{(246mn + 10m + 10n)/15,$
    $(1661771mn + 111248m + 136136n)/278460\}$

13. $SDD^{\#}(\text{NHC-TM-R}(m,n)) = \{(296mn - 6m - 6n)/3,$
    $(9760mn + 108m + 54n)/105\}$

14. $SO^{\#}(\text{NHC-TM-R}(m,n))$
    $= \{(16\sqrt{13} + 16\sqrt{5} + 66\sqrt{2})mn + (8\sqrt{2} - 8\sqrt{5})m$
    $+ (8\sqrt{2} - 8\sqrt{5})n, (40 + 148\sqrt{2} + 4\sqrt{85}$
    $+ 8\sqrt{113} + 4\sqrt{130} + 4\sqrt{145})mn + (4\sqrt{89} - 4\sqrt{113} + 4\sqrt{41}$
    $- 28\sqrt{2})m + (4\sqrt{74} - 4\sqrt{113} + 4\sqrt{41})n\}$

15. $HM^{\#}(\text{NHC-TM-R}(m,n)) = \{1480mn - 80m - 80n,$
    $11252mn - 684m - 900n\}$

3.2. Multiplicative Self-Powered Molecular Descriptors. In this section, the scalar multiplicative self-powered molecular descriptors based on the bond classification for the MOFs mentioned in Tables 1–4 are derived from the following equations by setting the unit weight for the atom and bonds. For MOF $\in \{\text{PTC-TM-H}(q), \text{PTC-TM-P}(q,r), \text{NHC-TM-R}(m,n)\}$

$$\Psi^{dp*}(\text{MOF}) = d(2,2)\Psi(2,2)^{\Psi(2,2)} \times d(2,3)\Psi(2,3)^{\Psi(2,3)} \times d(3,3)\Psi(3,3)^{\Psi(3,3)} \times d(2,4)\Psi(2,4)^{\Psi(2,4)}$$

For MOF $\in \{\text{PTC-TM-H}(q), \text{PTC-TM-P}(q,r)\}$

Table 7. Entropy Values Induced from Degree and Degree-Sum Descriptors for NHC-TM-R(m,m)

f		$m = 2$	$m = 3$	$m = 4$	$m = 5$	$m = 6$	$m = 7$	$m = 8$	$m = 9$	$m = 10$
M_1	d	6.867	7.714	8.305	8.758	9.128	9.439	9.708	9.945	10.157
	s	7.750	8.667	9.282	9.748	10.124	10.439	10.711	10.950	11.163
M_2	d	7.172	8.025	8.618	9.073	9.443	9.755	10.025	10.262	10.475
	s	9.025	9.988	10.619	11.092	11.473	11.791	12.065	12.305	12.519
ABC	d	4.737	5.594	6.191	6.648	7.019	7.332	7.602	7.839	8.052
	s	4.209	5.130	5.759	6.235	6.618	6.938	7.213	7.455	7.670
R	d	4.052	4.932	5.539	6.002	6.376	6.690	6.961	7.200	7.413
	s	2.208	3.416	4.189	4.745	5.177	5.530	5.828	6.086	6.313
GA	d	5.125	5.970	6.560	7.014	7.383	7.694	7.963	8.200	8.412
	s	5.047	5.930	6.538	7.002	7.378	7.693	7.965	8.204	8.417
AZ	d	7.427	8.266	8.852	9.303	9.670	9.980	10.248	10.484	10.696
	s	9.390	10.364	10.999	11.475	11.856	12.175	12.450	12.691	12.905
ReZ_3	d	8.876	9.749	10.350	10.809	11.181	11.495	11.765	12.004	12.216
	s	11.641	12.685	13.345	13.831	14.219	14.541	14.818	15.060	15.276
SC	d	4.209	5.085	5.690	6.152	6.525	6.840	7.111	7.349	7.562
	s	3.339	4.359	5.038	5.542	5.942	6.273	6.556	6.803	7.022
RRR	d	5.683	6.532	7.125	7.580	7.951	8.263	8.533	8.770	8.982
	s	6.942	7.841	8.451	8.915	9.289	9.604	9.876	10.115	10.328
ISI	d	5.443	6.291	6.882	7.337	7.707	8.019	8.288	8.526	8.738
	s	6.403	7.291	7.897	8.360	8.734	9.049	9.320	9.559	9.772
F	d	7.899	8.766	9.364	9.822	10.194	10.507	10.778	11.016	11.229
	s	9.694	10.677	11.314	11.791	12.173	12.492	12.766	13.007	13.221
H	d	4.037	4.917	5.523	5.985	6.359	6.674	6.945	7.183	7.396
	s	2.197	3.409	4.183	4.740	5.173	5.526	5.824	6.082	6.310
SDD	d	5.904	6.748	7.337	7.791	8.160	8.472	8.741	8.978	9.190
	s	5.803	6.670	7.269	7.727	8.098	8.411	8.681	8.918	9.131
SO	d	6.533	7.381	7.971	8.426	8.795	9.107	9.376	9.614	9.826
	s	7.422	8.330	8.942	9.406	9.781	10.096	10.368	10.607	10.820
HM	d	8.560	9.429	10.028	10.486	10.857	11.170	11.441	11.679	11.891
	s	10.344	11.348	11.993	12.473	12.856	13.177	13.452	13.693	13.908

$$\Psi^{sp*}(\text{MOF}) = s(4,5)\Psi(4,5)^{\Psi(4,5)} \times s(5,8)\Psi(5,8)^{\Psi(5,8)}$$
$$\times s(7,8)\Psi(7,8)^{\Psi(7,8)} \times s(8,8)\Psi(8,8)^{\Psi(8,8)}$$
$$\times s(8,9)\Psi(8,9)^{\Psi(8,9)} \times s(9,9)\Psi(9,9)^{\Psi(9,9)}$$

and MOF = NHC-TM-R(m,n)

$$\Psi^{sp*}(\text{MOF}) = s(4,5)\Psi(4,5)^{\Psi(4,5)} \times s(5,7)\Psi(5,7)^{\Psi(5,7)}$$
$$\times s(5,8)\Psi(5,8)^{\Psi(5,8)} \times s(6,7)\Psi(6,7)^{\Psi(6,7)}$$
$$\times s(6,8)\Psi(6,8)^{\Psi(6,8)} \times s(7,7)\Psi(7,7)^{\Psi(7,7)}$$
$$\times s(7,8)\Psi(7,8)^{\Psi(7,8)} \times s(7,9)\Psi(7,9)^{\Psi(7,9)}$$
$$\times s(8,8)\Psi(8,8)^{\Psi(8,8)} \times s(8,9)\Psi(8,9)^{\Psi(8,9)}$$
$$\times s(9,9)\Psi(9,9)^{\Psi(9,9)}$$

We denote $D = \{(2,2), (2,3), (3,3), (2,4)\}$, $S = \{(4,5), (5,8), (7,8), (8,8), (8,9), (9,9)\}$, and $S_1 = \{(4,5), (5,7), (5,8), (6,7), (6,8), (7,7), (7,8), (7,9), (8,8), (8,9), (9,9)\}$.

Let $\Psi_\alpha = \prod_{(q,r)\in D} \Psi(q,r)^{\Psi(q,r)}$, $\Psi_\beta = \prod_{(q,r)\in S} \Psi(q,r)^{\Psi(q,r)}$, and $\Psi_{\beta_1} = \prod_{(q,r)\in S_1} \Psi(q,r)^{\Psi(q,r)}$. Hence, we have the following expressions for three types of MOF structures.

1. $\Psi^{d*}(\text{PTC-TM-H}(q)) = \Psi_\alpha(2799360q^7 - 11664000q^6 + 20995200q^5 - 21306240q^4 + 13219200q^3 - 5028480q^2 + 1088640q - 103680)$

2. $\Psi^{d*}(\text{PTC-TM-P}(q,r)) = \Psi_\alpha(34560q^4r^3 - 23040q^4r^2 + 34560q^3r^4 - 63360q^3r^3 + 23040q^3r^2 - 23040q^2r^4 + 23040q^2r^3 - 5760q^2r^2)$

3. $\Psi^{d*}(\text{NHC-TM-R}(m,n)) = \Psi_\alpha(11264m^4n^3 - 5632m^4n^2 + 11264m^3n^4 - 11264m^3n^3 - 5632m^2n^4)$

4. $\Psi^{s*}(\text{PTC-TM-H}(q)) = \Psi_\beta(967458816q^{10} - 5482266624q^9 + 14108774400q^8 - 21767823360q^7 + 22332174336q^6 - 15936196608q^5 + 8017367040q^4 - 2809810944q^3 + 656916480q^2 - 92565504q + 5971968)$

5. $\Psi^{s*}(\text{PTC-TM-P}(q,r)) = \Psi_\beta(1327104q^6r^4 - 884736q^6r^3 + 2654208q^5r^5 - 3981312q^5r^4 + 1327104q^5r^3 + 1327104q^4r^6 - 3981312q^4r^5 + 2985984q^4r^4 - 663552q^4r^3 - 884736q^3r^6 + 1327104q^3r^5 - 663552q^3r^4 + 110592q^3r^3)$

6. $\Psi^{s*}(\text{NHC-TM-R}(m,n)) = \Psi_{\beta_1}(37748736m^{10}n^9 - 50331648m^{10}n^8 + 12582912m^{10}n^7 + 37748736m^9n^{10} - 75497472m^9n^9 + 37748736m^9n^8 - 25165824m^8n^{10} + 25165824m^8n^9)$

3.3. Numerical Computations of Entropies. In this section, we present the numerical entropy values of three MOFs discussed in the earlier sections based on the degree/degree-sum topological functions. For the parallelogram and rectangular types of MOFs, we discuss the cases of PTC-TM-P(q,q) and NHC-TM-R(m,m). The results of these frameworks entropy values are shown in Tables 5−7 and presented in Figure 5. The graph entropies increase in the order H, R, SC, ABC, GA, ISI, RRR, SDD, SO, M_1, M_2, AZ, F, HM, ReZ_3 for degree descriptors of all three MOFs, and in the case of degree-sum descriptors, the same trend continues except for SDD, which moves forward before two descriptors.
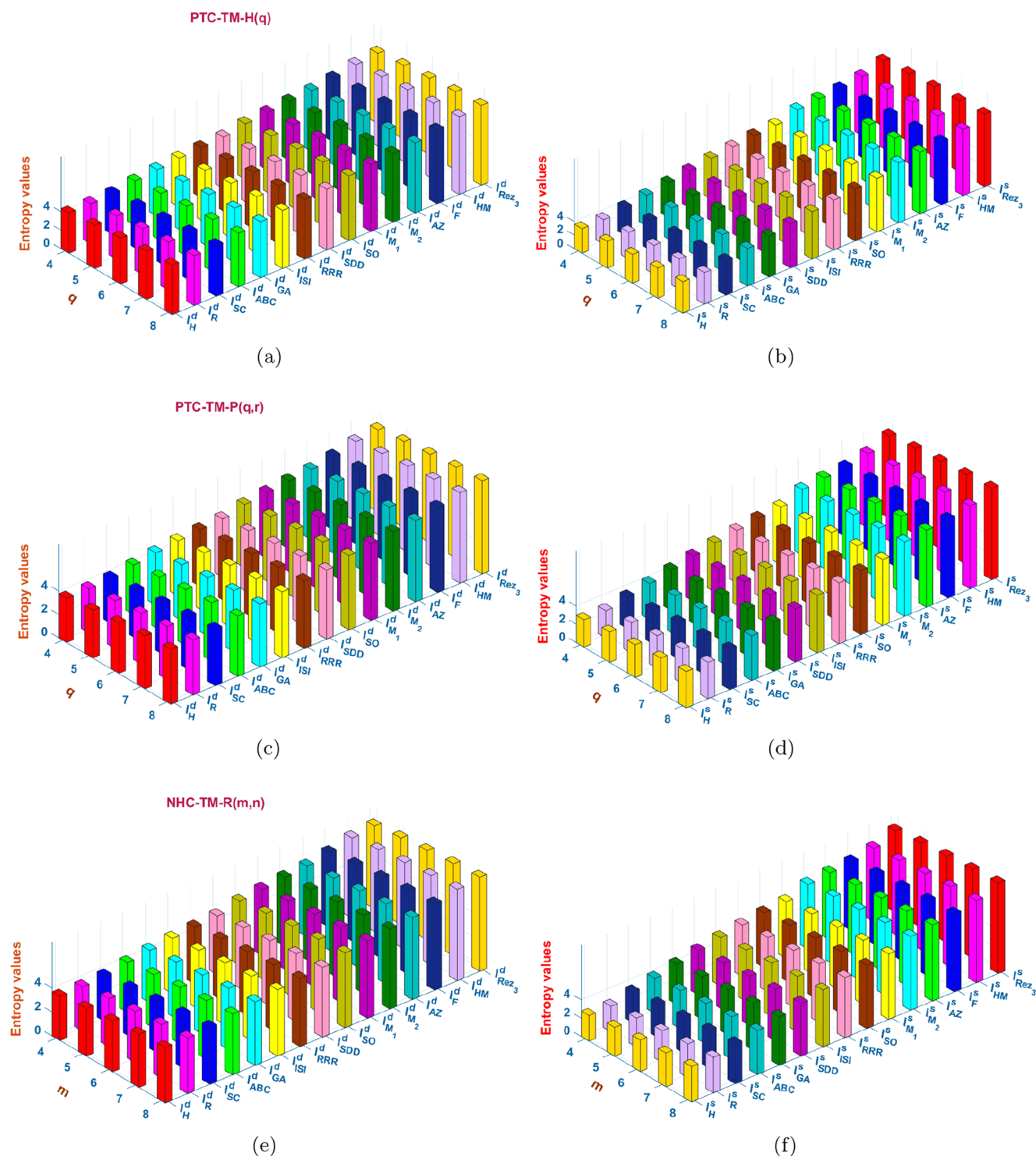
Figure 5. Comparative analysis of degree and degree-sum entropies (a,b) PTC-TM-H(q), (c,d) PTC-TM-P(q,q), and (e,f) NHC-TM-R(m,m).

4. NMR AND ESR SPECTRAL PREDICTIONS OF THREE STRUCTURES OF CORONENE-BASED METAL ORGANIC FRAMEWORKS

Bloom et al.[53] introduced the concept of distance status sequence and the distance degree sequence vector (DDSV) which can shed light on the first level vertex partitioning of complex networks such as coronene-based metal organic frameworks. The DDSV is defined as a p-tuple vector (d_{i0}, d_{i1}, d_{i2}, ..., d_{ij}, ... d_{ip}) in which d_{ij} is the number of vertices located at a distance j from a vertex v_i of the coronene-based transition metal organic frameworks. In the present study, the DDSV is invoked to partition the vertices, in addition to using the chemical identity of the vertex and symmetries of the three networks shown in Figures 2−4. In this method, we use TopoChemie-2020 software[52] to compute the number of vertices at a given distance from the vertex v_i by making use of the distance matrices generated by the codes. Hence we can assign a DDSV

Table 8. Vertex Equivalence Classes of the Three Coronene-Based Metal Organic Frameworks in Figures 2−4 Together with Their Number of ^{13}C and Proton NMR Signals for Each MOF

| coronene-based MOF types	molecular formulas	nuclear equivalence classes	^{13}C NMR signals and intensity patterns	proton NMR signals and intensity patterns
hexagonal (Figure 2): PTC-TM-H(3)	$M_{72}S_{228}C_{456}$	$M(6^4\ 12^4)$ $S(12^{19})$ $C(6^{10}\ 12^{33})$	43 1:1:⋯:1(10) 2:2:⋯:2(33)	
parallogram (Figure 3): PTC-TM-P(3,4)	$M_{49}S_{144}C_{288}$	$M(1\ 2^{24})$ $S(2^{72})$ $C(2^{144})$	144 1:1:⋯:1(144)	
rectangular (Figure 4): NHC-TM-R(3,5)	$M_{38}N_{120}C_{360}H_{180}$	$M(2^5\ 4^7)$ $N(4^{30})$ $C(2^6\ 4^{87})$ $H{-}N\ (4^{30})$ $H{-}C\ (4^{15})$	93 1:1:⋯:1(6) 2:2:⋯:2(87)	$H{-}N\ (30)$ 1:1:⋯:1(30) $H{-}C\ (15)$ 1:1:⋯:1(15)

for each vertex of the coronene-based metal organic framework under consideration. Then the code analyzes the DDSVs assigned to each vertex, and if the vertices carry the same DDSV, they are grouped into the same set. Subsequently, the chemical identity of each element in the MOF and the automorphism symmetry of the structures[54,55] are further invoked in order to arrive at the equivalence classes of the vertices of the MOFs, as shown in Table 8.

In Table 8, we show the vertex equivalence classes of the three coronene-based metal organic frameworks shown in Figures 2−4 together with their number of ^{13}C and proton NMR signals for each MOF. As can be seen from Table 8, the three structures of coronene-based metal organic frameworks all exhibit contrasting nuclear equivalence classes on the basis of their differing automorphic symmetries, connectivities, and nuclear identities. The three structures also exhibit sufficiently contrasting carbon nuclear equivalence classes, and thus, ^{13}C NMR spectroscopy should be a powerful tool to contrast them. As can be seen from Table 8, the number of ^{13}C NMR signals and their intensity patterns can be predicted from the structures of the nuclear equivalence classes. Likewise there are two types of proton NMR spectral patterns predicted for the rectangular structure depending on whether the proton is attached to carbon or nitrogen. On that basis and DDSV patterns, the N−H protons yield 30 signals with equal intensity ratios while the C−H protons result in a pattern of 15 signals with equal intensities. Likewise, the other nuclear NMR patterns can also be predicted from Table 8 depending on the isotope and its nuclear spin quantum number. More detailed operator theoretical methods were formulated earlier[56] for the construction of symmetry-adapted nuclear spin functions involving different spin quantum numbers, and as this is a separate topic, we shall not dwell deep into the details of NMR Hamiltonian analysis.

The equivalence classes enumerated in Table 8 can also be powerful in the generation of ESR hyperfine structures of the associated radicals arising from the coupling of an unpaired electron with the nuclear isotope possessing nonzero nuclear spin. For the sake of demonstration, we consider the hyperfine structures arising from the coupling of the unpaired electron with ^{13}C nuclear spins in the three TM-MOFs considered here. The combinatorial method to generate the ESR hyperfine patterns from the nuclear equivalence classes involves generating function methods[56,57] which have been well described in the cited references in extensive details. Hence we shall not repeat the extensive formalisms here. Briefly the generating function methods

yield the various spin function distributions, and the coefficients in the generating functions yield the relative intensities in the spectra as they represent the spin populations with the given spin function distribution. Figure 6 shows three panels a−c, which display the ESR hyperfine patterns arising from the coupling of an unpaired electron with ^{13}C nuclei for the 3 structures shown in Figures 2−4, respectively. The patterns are for the illustrative purposes only, as the actual experimental ESR hyperfine structures would depend on the geometrical distance of the unpaired electron from each equivalence class of ^{13}C nuclei. Evidently the ^{13}C nuclei in the equivalence class closest to the unpaired electron would interact strongest, and thus those nuclei will contribute to a greater extent to the ESR hyperfine structure compared to those equivalence classes that are farthest from the unpaired electron. The spectra predicted here for the three structures with different topologies clearly show sufficient contrast that our predictions would aid experimental spectroscopists and synthetic chemists in their structure elucidations of transition-metal-based MOFs. Furthermore, these machine-generated spectral techniques become an integral part of computer-assisted structure elucidations[55] and machine learning methods for the spectra, which are becoming important components of artificial intelligence techniques in chemical applications.

The computed topological properties and the matrices that were computed in the process can also be quite useful in quantum chemical parametrizations for the hybrid quantum chemical techniques that are more suitable for such large systems. For example, the π-electrons can be treated quite well using an integration of graph theory with the Pariser−Parr−Pople methods.[58] For both σ and π electrons, one could employ the CASSCF/CI techniques[59] on a library of smaller building blocks of molecules in order to derive the parameters for the hybrid techniques that can then be used for the larger coronene-based transition metal organic frameworks. Consequently, distance-based topological indices including those based on resistance distances can provide significant simplifications and insights into deriving parameters from more accurate quantum chemical methods. Experimentally observable phase transitions in materials such as metal organic frameworks are often accompanied by topological changes from one structure to the other. In such cases, dynamical changes to the underlying structures can be readily characterized by topological reaction graphs called isomerization or reaction graphs as demonstrated for dynamic stereochemistry in organic molecules exhibiting internal dynamics.[60]
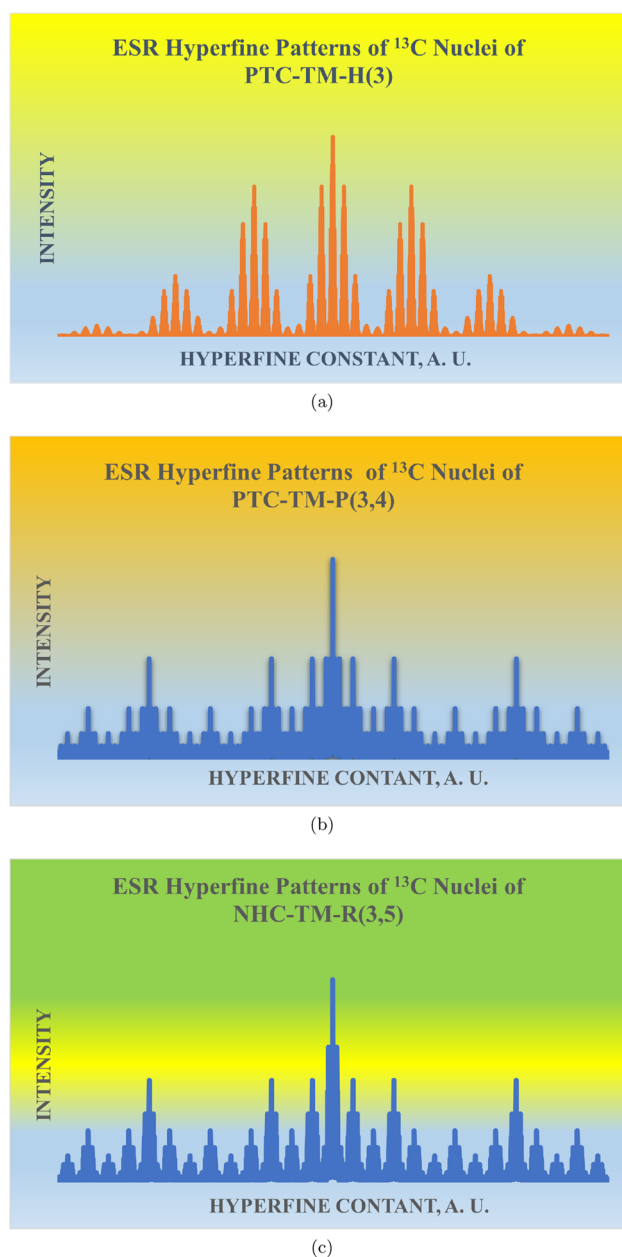
Figure 6. ESR hyperfine pattern arising from coupling with ^{13}C nuclei nuclei of (a) PTC-TM-H(3), (b) PTC-TM-P(3,4), and (c) NHC-TM-R(3,5).

5. CONCLUSION

We have discussed three different stackings of novel transition-metal-based MOFs with perthiolated coronene and −NH substituted coronene as linkers and analyzed their topological behaviors through degree- and degree-sum-based structural descriptors. The entropy metrics of these MOFs are also manifested by computing the scalar multiplicative self-exponential index functions. As the MOFs considered in this study belong to a larger class of partial cubes, the existing graph-theoretical techniques pose limitations for the evaluation of distance-based topological metrics and hence need to be revamped for deriving their distance-based entropies. On the other side, we have employed the distance degree vector sequences together with the automorphic symmetry of MOFs and the chemical identities of different atoms in the TM-MOFs

to produce the NMR and ESR spectroscopic signatures. Consequently, the developed techniques could become integral parts of chemical applications of artificial intelligence and machine learning for structure elucidation and spectral signatures, thus holding considerable promise in the future. Likewise, phase transitions and other critical phenomena in these structures are often accompanied by topological and morphological changes that are best characterized by changes to the topologies of the underlying networks. Hence, the techniques considered here are expected to find applications in the structures, dynamics, and spectroscopy of such transition metal organic frameworks. The ability of MOFs to modify their structure based on the required functionality and the invariant attribute of the topological descriptors emphasizes the importance of the derived results in understanding the topological and spectroscopic properties of these frameworks, thereby facilitating the design and synthesis of stable spintronic and biocompatible devices.

■ AUTHOR INFORMATION

Corresponding Author

Micheal Arockiaraj − *Department of Mathematics, Loyola College, Chennai 600034, India;* ● orcid.org/0000-0002-4457-1046; Email: marockiaraj@gmail.com

Authors

Zahid Raza − *Department of Mathematics, College of Sciences, University of Sharjah, Sharjah 27272, United Arab Emirates*

Aravindan Maaran − *Department of Mathematics, Loyola College, Chennai 600034, India*

S. Ruth Julie Kavitha − *Department of Mathematics, Loyola College, Chennai 600034, India*

Krishnan Balasubramanian − *School of Molecular Sciences, Arizona State University, Tempe, Arizona 85287-1604, United States*

Complete contact information is available at:
https://pubs.acs.org/10.1021/acsomega.3c00825

Notes

The authors declare no competing financial interest.

■ REFERENCES

(1) Safaei, M.; Foroughi, M. M.; Ebrahimpoor, N.; Jahani, S.; Omidi, A.; Khatami, M. A review on metal-organic frameworks: Synthesis and applications. *Trends Anal. Chem.* **2019**, *118*, 401−425.

(2) Barthel, S.; Alexandrov, E. V.; Proserpio, D. M.; Smit, B. Distinguishing metal-organic frameworks. *Cryst. Growth Des.* **2018**, *18*, 1738−1747.

(3) Zhou, H. C.; Long, J. R.; Yaghi, O. M. Introduction to metal-organic frameworks. *Chem. Rev.* **2012**, *112*, 673−674.

(4) Ahmed, I.; Jhung, S. H. Composites of metal-organic frameworks: Preparation and application in adsorption. *Mater. Today* **2014**, *17*, 136−146.

(5) McGrath, D. T.; Ryan, M. D.; MacInnis, J. J.; VandenBoer, T. C.; Young, C. J.; Katz, M. J. Selective decontamination of the reactive air pollutant nitrous acid via node-linker cooperativity in a metal-organic framework. *Chem. Sci.* **2019**, *10*, 5576−5581.

(6) Kim, K. C. Design strategies for metal-organic frameworks selectively capturing harmful gases. *J. Organomet. Chem.* **2018**, *854*, 94−105.

(7) Wang, H.; Zhu, Q.-L.; Zou, R.; Xu, Q. Metal-organic frameworks for energy applications. *Chem.* **2017**, *2*, 52−80.

(8) Lin, R.-B.; Xiang, S.; Xing, H.; Zhou, W.; Chen, B. Exploration of porous metal-organic frameworks for gas separation and purification. *Coord. Chem. Rev.* **2019**, *378*, 87−103.

(9) Stassen, I.; Burtch, N.; Talin, A.; Falcaro, P.; Allendorf, M.; Ameloot, R. An updated roadmap for the integration of metal-organic frameworks with electronic devices and chemical sensors. *Chem. Soc. Rev.* **2017**, *46*, 3185−3241.

(10) Zhang, X.; Chen, Z.; Liu, X.; Hanna, S. L.; Wang, X.; Taheri-Ledari, R.; Maleki, A.; Li, P.; Farha, O. K. A historical overview of the activation and porosity of metal-organic framework. *Chem. Soc. Rev.* **2020**, *49*, 7406−7427.

(11) Yap, M. H.; Fow, K. L.; Chen, G. Z. Synthesis and applications of MOF-derived porous nanostructures. *Green Energy Environ.* **2017**, *2*, 218−245.

(12) Nik Zaiman, N. F. H.; Shaari, N.; Harun, N. A. M. Developing metal-organic framework-based composite for innovative fuel cell application: An overview. *Int. J. Energy Res.* **2022**, *46*, 471−504.

(13) Bieniek, A.; Terzyk, A. P.; Wiśniewski, M.; Roszek, K.; Kowalczyk, P.; Sarkisov, L.; Keskin, S.; Kaneko, K. MOF materials as therapeutic agents, drug carriers, imaging agents and biosensors in cancer biomedicine: Recent advances and perspectives. *Prog. Mater. Sci.* **2021**, *117*, 100743.

(14) Zhang, T.; Lin, W. Metal-organic frameworks for artificial photosynthesis and photocatalysis. *Chem. Soc. Rev.* **2014**, *43*, 5982−5993.

(15) Fan, W. K.; Tahir, M. Recent advances on cobalt metal organic frameworks (MOFs) for photocatalytic CO_2 reduction to renewable energy and fuels: A review on current progress and future directions. *Energy Convers. Manag.* **2022**, *253*, 115180.

(16) Lopez, Y. C.; Viltres, H.; Gupta, N. K.; Acevedo-Pena, P.; Leyva, C.; Ghaffari, Y.; Gupta, A.; Kim, S.; Bae, J.; Kim, K. S. Transition metal-based metal-organic frameworks for environmental applications: A review. *Environ. Chem. Lett.* **2021**, *19*, 1295−1334.

(17) Dong, R.; Pfeffermann, M.; Skidin, D.; Wang, F.; Fu, Y.; Narita, A.; Tommasini, M.; Moresco, F.; Cuniberti, G.; Berger, R.; Müllen; Feng, K. X. Persulfurated coronene a new generation of sulflower. *J. Am. Chem. Soc.* **2017**, *139*, 2168−2171.

(18) Dong, R.; Zhang, Z.; Tranca, D. C.; Zhou, S.; Wang, M.; Adler, P.; Liao, Z.; Liu, F.; Sun, Y.; Shi, W.; Zhang, Z.; Zschech, E.; Mannsfeld, S. C. B.; Felser, C.; Feng, X. A Coronene-based semiconducting two-dimensional metal-organic framework with ferromagnetic behavior. *Nat. Commun.* **2018**, *9*, 2637.

(19) Dietl, T.; Ohno, H. Dilute ferromagnetic semiconductors: Physics and spintronic structures. *Rev. Mod. Phys.* **2014**, *86*, 187.

(20) Wang, J.; Wang, J.; Song, X.; Qi, S.; Zhao, M. Multifunctional electrocatalytic activity of coronene-based two-dimensional metal-organic frameworks: TM-PTC. *Appl. Surf. Sci.* **2020**, *511*, 145393.

(21) Chakravarty, C.; Mandal, B.; Sarkar, P. Coronene-based metal-organic framework: A theoretical exploration. *Phys. Chem. Chem. Phys.* **2016**, *18*, 25277−25283.

(22) Gonzalez-Diaz, H.; Vilar, S.; Santana, L.; Uriarte, E. Medicinal chemistry and bioinformatics-current trends in drugs discovery with networks topological indices. *Curr. Top. Med. Chem.* **2007**, *7*, 1015−1029.

(23) Todeschini, R.; Consonni, V. *Handbook of Molecular Descriptors for Chemoinformatics*; Wiley-VCH: Weinheim, Germany, 2009.

(24) Dearden, J. C. The use of topological indices in QSAR and QSPR modeling. *Adv. QSAR Model.* **2017**, *24*, 57−88.

(25) Rakić, M.; Furtula, B. A novel method for measuring the structure sensitivity of molecular descriptors. *J. Chemom.* **2019**, *33*, e3138.

(26) Arockiaraj, M.; Paul, D.; Klavžar, S.; Clement, J.; Tigga, S.; Balasubramanian, K. Relativistic distance based and bond additive topological descriptors of zeolite RHO materials. *J. Mol. Struct.* **2022**, *1250*, 131798.

(27) Hayat, S.; Khan, S.; Imran, M. Quality testing of spectrum-based distance descriptors for polycyclic aromatic hydrocarbons with applications to carbon nanotubes and nanocones. *Arab. J. Chem.* **2021**, *14*, 102994.

(28) Kavitha, S. R. J.; Abraham, J.; Arockiaraj, M.; Jency, J.; Balasubramanian, K. Topological characterization and graph entropies of tessellations of kekulene structures: Existence of isentropic structures and applications to thermochemistry, nuclear magnetic resonance, and electron spin resonance. *J. Phys. Chem. A* **2021**, *125*, 8140−8158.

(29) Rada, J. Exponential vertex-degree-based topological indices and discrimination. *MATCH Commun. Math. Comput. Chem.* **2019**, *82*, 29−41.

(30) Abraham, J.; Arockiaraj, M.; Jency, J.; Kavitha, S. R. J.; Balasubramanian, K. Graph entropies, enumeration of circuits, walks and topological properties of three classes of isoreticular metal organic frameworks. *J. Math. Chem.* **2022**, *60*, 695−732.

(31) Mondal, S.; De, N.; Pal, A. Topological indices of some chemical structures applied for the treatment of COVID-19 patients. *Polycycl. Aromat. Compd.* **2022**, *42*, 1220−1234.

(32) Öhrström, L. Let's talk about MOFs-topology and terminology of metal-organic frameworks and why we need them. *Crystals* **2015**, *5*, 154−162.

(33) Liu, J.-B.; Raza, Z.; Javaid, M. Zagreb connection numbers for cellular neural networks. *Discrete Dyn. Nat. Soc.* **2020**, *2020*, 8038304.

(34) Raza, Z. The harmonic and second Zagreb indices in random polyphenyl and spiro chains. *Polycycl. Aromat. Compd.* **2022**, *42*, 671−680.

(35) Javaid, M.; Javed, S.; Alanazi, Y. F.; Alanazi, A. M. Computing correlation among the graphs under lexicographic product via Zagreb indices. *J. Chem.* **2021**, *2021*, 7465171.

(36) Gutman, I.; Furtula, B.; Katanić, V. Randić index and informations. *AKCE Int. J. Graphs Comb.* **2018**, *15*, 307−312.

(37) Ke, X.; Wei, S.; Huang, J. The atom-bond connectivity and geometric arithmetic indices in random polyphenyl chains. *Polycycl. Aromat. Compd.* **2021**, *41*, 1873−1882.

(38) Gao, W.; Siddiqui, M. K.; Imran, M.; Jamil, M. K.; Farahani, M. R. Forgotten topological index of chemical structure in drugs. *Saudi Pharm. J.* **2016**, *24*, 258−264.

(39) Ali, A.; Elumalai, S.; Mansour, T. On the symmetric division deg index of molecular graphs. *MATCH Commun. Math. Comput. Chem.* **2020**, *83*, 205−220.

(40) Cruz, R.; Gutman, I.; Rada, J. Sombor index of chemical graphs. *Appl. Math. Comput.* **2021**, *399*, 126018.

(41) Ali, A.; Bhatti, A. A.; Raza, Z. Some vertex-degree-based topological indices of polyomino chains. *J. Comput. Theor. Nanosci.* **2015**, *12*, 2101−2107.

(42) Dehmer, M.; Mowshowitz, A. A history of graph entropy measures. *Inf. Sci.* **2011**, *181*, 57−78.

(43) Manzoor, S.; Siddiqui, M. K.; Ahmad, S. On entropy measures of molecular graphs using topological indices. *Arab. J. Chem.* **2020**, *13*, 6285−6298.

(44) Tan, Y. J.; Wu, J. Network structure entropy and its application to scale-free networks. *Syst. Eng. Theory Pract.* **2004**, *24*, 1−3.

(45) Jacob, K.; Clement, J.; Arockiaraj, M.; Paul, D.; Balasubramanian, K. Topological characterization and entropy measures of tetragonal zeolite merlinoites. *J. Mol. Struct.* **2023**, *1277*, 134786.

(46) Arockiaraj, M.; Jency, J.; Abraham, J.; Ruth Julie Kavitha, S.; Balasubramanian, K. Two-dimensional coronene fractal structures: Topological entropy measures, energetics, NMR and ESR spectroscopic patterns and existence of isentropic structures. *Mol. Phys.* **2022**, *120*, e2079568.

(47) Ashraful Alam, Md.; Ghani, M. U.; Kamran, M.; Shazib Hameed, M.; Hussain Khan, R.; Baig, A. Q. Degree-based entropy for a non-kekulean benzenoid graph. *Comput. Theor. Chem.* **2022**, *2022*, 2288207.

(48) Julietraja, K.; Venugopal, P.; Prabhu, S.; Arulmozhi, A. K.; Siddiqui, M. K. Structural analysis of three types of PAHs using entropy measures. *Polycycl. Aromat. Compd.* **2022**, *42*, 4101−4131.

(49) Paul, D.; Arockiaraj, M.; Tigga, S.; Balasubramanian, K. Zeolite AST: Relativistic degree and distance based topological descriptors. *Comput. Theor. Chem.* **2022**, *1218*, 113933.

(50) Arockiaraj, M.; Paul, D.; Klavžar, S.; Clement, J.; Tigga, S.; Balasubramanian, K. Relativistic topological and spectral characteristics of zeolite SAS structures. *J. Mol. Struct.* **2022**, *1270*, 133854.

(51) Shannon, C. E.; Weaver, W. *The Mathematical Theory of Communication*; UI Press: Champagne, IL, 1949.

(52) Balasubramanian, K. *TopoChemie-2020*, A Computational Package for Computing Topological Indices, Spectral Polynomials, Walks and Distance Degree Sequences and Combinatorial Generators, 2020.

(53) Bloom, G. S.; Kennedy, J. W.; Quintas, L. V. Some Problems Concerning Distance and Path Degree Sequences. In *Graph Theory*; Borowiecki, M., Kennedy, J. W., Syslo, M. M., Eds.; Lecture Notes in Mathematics; Springer: Berlin, Germany, 1983; Vol. *1018*, pp 179−190.

(54) Balasubramanian, K. Symmetry groups of chemical graphs. *Int. J. Quantum Chem.* **1982**, *21*, 411−418.

(55) Liu, X.; Balasubramanian, K.; Munk, M. E. Computer-assisted graph-theoretical construction of ^{13}C NMR signal and intensity patterns. *J. Magn. Reson.* **1990**, *87*, 457−474.

(56) Balasubramanian, K. Operator and algebraic methods for NMR spectroscopy. I. Generation of NMR spin species. *J. Chem. Phys.* **1983**, *78*, 6358.

(57) Balasubramanian, K. Symmetry, combinatorics. *artificial intelligence, music and spectroscopy. Symmetry* **2021**, *13*, 1850.

(58) Balasubramanian, K. Graph theory and the PPP method. *J. Math. Chem.* **1991**, *7*, 353−362.

(59) Balasubramanian, K. CASSCF/CI calculations on Si_4 and Si_4^+. *Chem. Phys. Lett.* **1987**, *135*, 283−287.

(60) Balasubramanian, K. Enumeration of internal-rotation reactions and their reaction graphs. *Theor. Chim. Acta.* **1979**, *53*, 129−146.

■ NOTE ADDED AFTER ASAP PUBLICATION

This paper originally published ASAP on March 29, 2023. Due to a production error, several mistakes needed correcting on page E. A new version reposted on March 31, 2023.